Wang et al. Nanoscale Research Letters (2016) 11:316
DOI 10.1186/s11671-016-1540-4

Nanoscale Research Letters

NANO EXPRESS Open Access

Enhanced performance of $CH_3NH_3PbI_{3-x}Cl_x$ perovskite solar cells by CH_3NH_3I modification of TiO_2-perovskite layer interface

Wen Wang[1], Zongbao Zhang[1], Yangyang Cai[1], Jinshan Chen[1], Jianming Wang[1], Riyan Huang[1], Xubing Lu[1], Xingsen Gao[1], Lingling Shui[2], Sujuan Wu[1*] and Jun-Ming Liu[1,3]

Abstract

In this work, perovskite solar cells (PSCs) with $CH_3NH_3PbI_{3-x}Cl_x$ as active layer and spiro-OMeTAD as hole-transport media have been fabricated by one-step method. The methylammonium iodide (CH_3NH_3I) solution with different concentrations is used to modify the interface between mesoporous TiO_2 (meso-TiO_2) film and $CH_3NH_3PbI_{3-x}Cl_x$ perovskite layer. Several techniques including X-ray diffraction, scanning electron microscopy, optical absorption, electrochemical impedance spectroscopy (EIS) and photoluminescence are used to investigate the effect of the interfacial modification. It is found that the interfacial modification by CH_3NH_3I enhance the crystallinity and increase the grain size of $CH_3NH_3PbI_{3-x}Cl_x$ layer, and improve the surface wetting properties of perovskite precursor on meso-TiO_2 film. The sunlight absorption and external quantum efficiency of PSCs in the visible region with wavelength less than 600 nm have been improved. The Nyquist plots obtained from the EIS suggest that the CH_3NH_3I modification can reduce the charge recombination rates. The photoluminescence measurement shows that the exciton dissociation in the modified devices is more effective than that in the control samples. The photovoltaic performance of the modified devices can be significantly improved with respect to the reference (control) devices. The CH_3NH_3I modified devices at the optimized concentration demonstrate the average power conversion efficiency of 12.27 % in comparison with the average efficiency of 9.68 % for the reference devices.

Keywords: CH_3NH_3I, Interfacial modification, $CH_3NH_3PbI_{3-x}Cl_x$ perovskite solar cells, Photoelectronic properties, Performance

Background

Recently, solar cells based on composites of organometallic halide perovskite have attracted much attention due to their super high absorption coefficients, relatively high carrier mobility and easy fabrication by solution process [1–3]. The efficiency of perovskite ($CH_3NH_3PbX_3$, $X = Cl$, Br, I)-based photovoltaic devices has greatly increased from 3.8 % to more than 20 % in just a few years [4–6]. It is well known that the microstructure and crystallinity of perovskite layer have important influence on the performance of perovskite solar cells (PSCs) [7]. The morphology of the perovskite films influences on exciton separation, charge transfer, and recombination [8]. The low crystallinity of the perovskite films will result in a strong leakage path and has a negative effect on the charge dynamics of PSCs [5, 9]. However, a precise control of the morphology and crystallinity of perovskite layer remains a critical challenge due to the complex crystal growth mechanism of the perovskite materials. Substantial effort has been done to improve the microstructure of PSCs by adjusting the perovskite crystallization kinetics, such as additives modification [10], composition optimization [11], solvent extraction [12], and controlling the temperature, annealing time, or atmosphere [13–15]. However, a control of the crystalline property and

* Correspondence: sujwu@scnu.edu.cn
[1]Institute for Advanced Materials and Laboratory of Quantum Engineering and Quantum Materials, South China Normal University, Guangzhou 510006, China
Full list of author information is available at the end of the article

microstructure just by optimizing the fabrication processing seems to be insufficient.

It is known that surface modification has been widely used to improve the performance of organic solar cells and dye-sensitized solar cells [16–19]. Interfacial engineering has been also used as a new strategy to control the morphology of perovskite layer and improve the efficiency of PSCs. It is found that interfacial modification can significantly promote the charge transfer and reduce the recombination rate for those PSCs with metal oxides as electron transport materials [20–22]. It was reported that a modification of the interface between ZnO and perovskite layer using self-assembled monolayer can optimize the morphology of perovskite layer and improve the performance of PSCs [23, 24]. It was also demonstrated that modifying the TiO_2/$CH_3NH_3PbI_3$ heterojunction interface by glycine can enhance the photovoltaic performance of two-step solution-processed PSCs [25].

In addition, a modification of the perovskite/TiO_2 interface with a nanoscale layer of Al_2O_3 can reduce the charge losses of the PSCs [26]. Excess $CH_3NH_3^+$ or methylammonium iodide (CH_3NH_3I) is very important for the improvement in the optoelectronic properties of perovskite layer. Better coverage, uniform and pinhole-free perovskite films by adding excess $CH_3NH_3^+$ to the reactants of perovskite layer can be obtained [27]. During the preparation of perovskite layer by sequential deposition method, a proper addition of CH_3NH_3I to PbI_2 solution not only enhances the absorption but also reduces the recombination rate, resulting in the improvement of efficiency in PSCs [28]. These results suggest that it is promise to introduce CH_3NH_3I to modify the interface of PSCs.

Based on these considerations, in this work, the PSCs with the glass/FTO/compact TiO_2/meso-TiO_2/$CH_3NH_3PbI_{3-x}Cl_x$/spiro-OMeTAD/Ag structure are fabricated by the one-step solution method. Here, we choose CH_3NH_3I to modify the interface between meso-TiO_2 and $CH_3NH_3PbI_{3-x}Cl_x$ perovskite layer and investigate the effect of CH_3NH_3I concentration on the microstructure of $CH_3NH_3PbI_{3-x}Cl_x$ layer and photoelectronic properties of the PSCs. The related mechanism is addressed too. The results show that the CH_3NH_3I modification at the optimal concentration can improve the sunlight absorption and external quantum efficiency (EQE) in the visible region at the wavelengths less than 600 nm, reduce the charge recombination rate, and promote the charge transfer, resulting in the enhanced performance. The average power conversion efficiency (PCE) of the PSCs can be enhanced from 9.68 to 12.27 %, respectively.

Methods

Figure 1 shows a schematic diagram of the PSCs fabricated in this work. First, each pre-cleaned FTO substrate

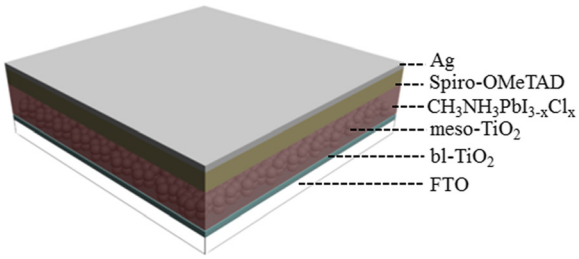

Fig. 1 (Color online) A schematic drawing of the perovskite device

was coated with a 60-nm TiO_2 blocking film by spinning a sol-gel solution (0.25 M titanium isopropoxide in ethanol) at 4000 rpm. The layer was annealed at 500 °C for 30 min to allow sufficient crystallization in ambient air. The meso-TiO_2 layer was deposited on the TiO_2 blocking film by spin-coating a TiO_2 solution (18NR-T, Dyesol) in ethanol at 6000 rpm. These samples were then sintered at 550 °C for 30 min in air to obtain meso-TiO_2 films. For every batch, several of the as-prepared samples were chosen as the reference samples and the other samples were submitted to next processing.

CH_3NH_3I was synthesized using the reported method [3]. For the CH_3NH_3I modification, the CH_3NH_3I of different concentration dissolved in isopropanol was spin-coated on the meso-TiO_2 films at 4000 rpm. The untreated samples were chosen as the references. After the modification, these samples together with the reference samples were annealed at 60 °C for 30 min. CH_3NH_3I and $PbCl_2$ (Aladdin, 99.5 %) were dissolved in *N*,*N*-dimethylformamide (Aladdin, 99.9 %) to obtain a 40 wt % precursor solution with a CH_3NH_3I:$PbCl_2$ molar ratio of 3:1. The solution was filtered with a 0.45-μm pore size filters before spin-coating. To fabricate the PSCs from the above samples, a $CH_3NH_3PbI_{3-x}Cl_x$ layer was deposited onto the meso-TiO_2 film by spin-coating a solution of $CH_3NH_3PbI_{3-x}Cl_x$ (40 wt % dissolved in DMF) at 2000 rpm for 30 s in the glove box. Then, these samples were annealed in nitrogen (N_2) ambient at 100 °C for 45 min. Subsequently, 0.08 M spiro-OMeTAD in chlorobenzene solution was spin-coated onto the perovskite film. These samples were left in dry air overnight in the dark. Finally, Ag electrodes with thickness of ~100 nm were evaporated on the sample surface through a shadow mask under a vacuum of 1×10^{-4} Pa. All the as-prepared PSCs were fabricated with the standard in-plane size of 3 mm × 4 mm.

Device Characterizations

The morphology and crystallinity of the perovskite layer were investigated using scanning electron microscopy (SEM, ZEISS ULTRA 55) and the X-ray diffraction (XRD) (X'Pert PRO, Cu Ká radiation). The photovoltaic

performance of these PSCs was characterized using a Keithley 2400 source meter under an illumination of 100 mW/cm^2 (Newport 91160, 150 W solar simulator equipped with an AM 1.5 G filter). The radiation intensity was calibrated by a standard silicon solar cell (certified by NREL) as the reference. The EQE and the UV-vis absorption spectra were measured using a standard EQE system (Newport 66902). The electrochemical impedance spectroscopy (EIS) measurements were performed on the Zahner Zennium electrochemical workstation in the dark. A 20-mV ac-sinusoidal signal source was employed over the constant bias with the frequency ranging from 1 Hz to 4 MHz. The photoluminescence spectra (PL) were measured by a fluorescence spectrophotometer (HITACHI F-5000) exited at 405 nm. The PL spectra have been normalized to the absorbance and measured in the same conditions.

Results and Discussion

It is known that the interfacial property has a significant influence on the photovoltaic properties of the PSCs. In this work, it is found that the performance of $CH_3NH_3PbI_{3-x}Cl_x$ PSCs are influenced remarkably by the concentration of CH_3NH_3I solution used to modify the interface between the meso-TiO_2 and $CH_3NH_3PbI_{3-x}Cl_x$. To investigate the effect of CH_3NH_3I on the performance of PSCs, CH_3NH_3I solutions of different concentration at 0, 5, 10, and 20 mg/ml were used, labeled as x (x = 0, 5, 10, 20). Initially, we investigated the effect of CH_3NH_3I modification on the crystalline structure of $CH_3NH_3PbI_{3-x}Cl_x$ perovskite materials. Figure 2a shows the XRD patterns of $CH_3NH_3PbI_{3-x}Cl_x$ layers deposited on the meso-TiO_2 film without and with modification by CH_3NH_3I solutions with different concentrations. The peaks at 14.10°, 28.47°, 43.27°, and 58.88° can be attributed to the (110), (220), (330), and (440) reflections of the perovskite crystalline structure, respectively [23]. The presence of these peaks indicates the successful conversion into the perovskite structure, similar to earlier reports [27, 29]. The intensity of all these perovskite diffraction peaks enhances after the CH_3NH_3I modification and attains the maximum at x = 10. Figure 2b shows the detailed information of the XRD patterns from 13° to 15°. It can be seen that the intensity of (110) characteristic peak increases with the concentration of CH_3NH_3I and attains the maximum at x = 10 and then decreases with the increase of CH_3NH_3I concentration. This implies that the crystallinity of $CH_3NH_3PbI_{3-x}Cl_x$ film increases upon the CH_3NH_3I modification [8]. The improved crystallinity and preferred growth in the (110) direction can be attributed to the excess of $CH_3NH_3^+$ which slows the crystallization rate of perovskite layer [27, 28].

The interfacial modification of CH_3NH_3I also plays a critical role in the morphology of perovskite layer. The top-view SEM images of $CH_3NH_3PbI_{3-x}Cl_x$ films deposited on meso-TiO_2 modified by CH_3NH_3I solutions with different concentrations are presented in Fig. 3. It can be seen that the pinholes decrease and the grain size of $CH_3NH_3PbI_{3-x}Cl_x$ increases upon the CH_3NH_3I modification, which will benefit to the performance improvement [9]. For high efficiency PSCs, pinhole-free perovskite films with high crystalline properties are very important. In this view, the enhanced crystalline property and morphology evolution after CH_3NH_3I modification may promise an improved device performance of PSCs, which will be discussed below. Figure 4 shows the contact angles of $CH_3NH_3PbI_{3-x}Cl_x$ precursor solution directly dropped on meso-TiO_2 with and without CH_3NH_3I modification. As seen in Fig. 4, the contact angle decreases with increasing CH_3NH_3I

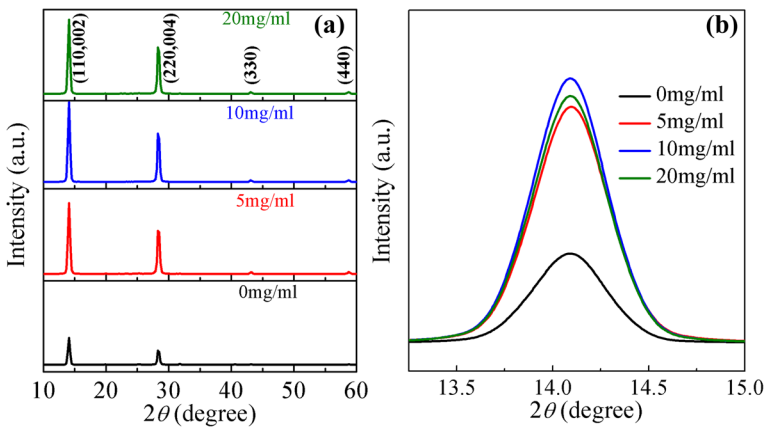

Fig. 2 (Color online) **a** X-ray diffraction (XRD) patterns of $CH_3NH_3PbI_{3-x}Cl_x$ perovskite layer. **b** Detail XRD information of $CH_3NH_3PbI_{3-x}Cl_x$ from 13° to 15°. The perovskite was deposited on meso-TiO_2 modified by CH_3NH_3I solutions with different concentrations

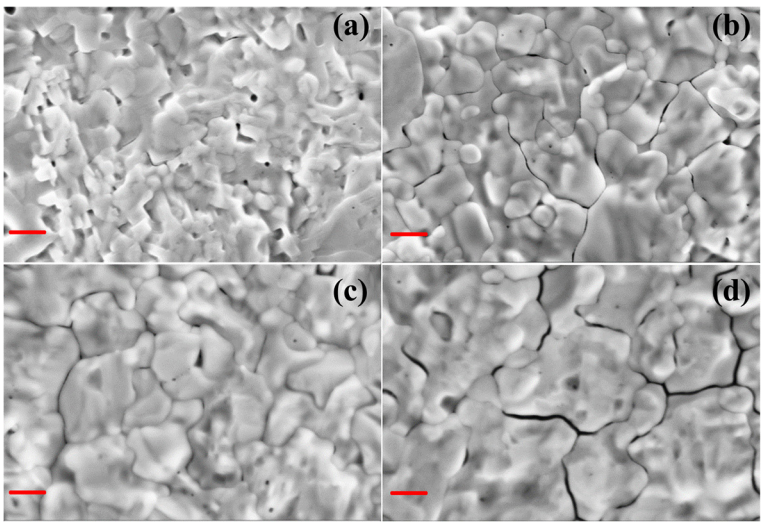

Fig. 3 (Color online) Top-view SEM images of the $CH_3NH_3PbI_{3-x}Cl_x$ films deposited on meso-TiO_2 films modified by CH_3NH_3I solutions with different concentrations **a** 0 mg/ml, **b** 5 mg/ml, **c** 10 mg/ml, and **d** 20 mg/ml, respectively. *Scale bar*, 500 nm

concentration. It implies that the surface wetting properties of perovskite precursor on meso-TiO_2 film are improved after the CH_3NH_3I modification, which will facilitate to improve the coverage rates of perovskite layer [30].

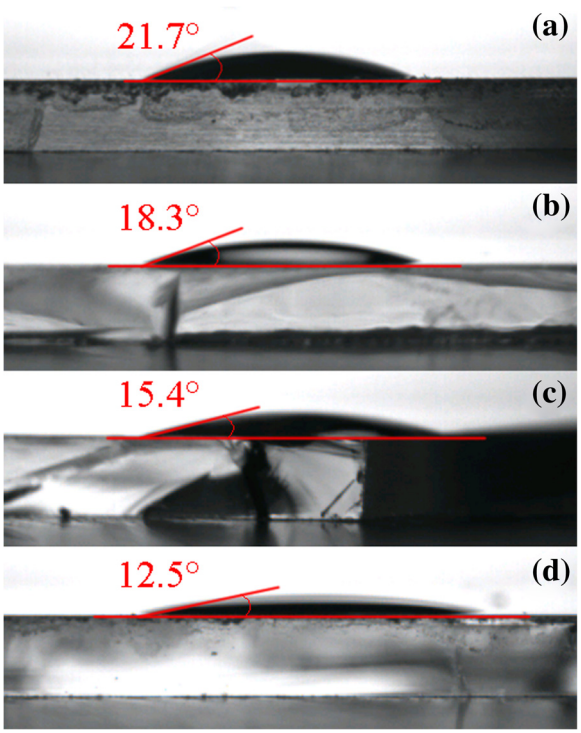

Fig. 4 (Color online) Contact angle of perovskite droplet on the meso-TiO_2 films modified by CH_3NH_3I solutions with different concentrations **a** 0 mg/ml, **b** 5 mg/ml, **c** 10 mg/ml, and **d** 20 mg/ml, respectively

To investigate the effect of CH_3NH_3I modification on the performance of PSCs, the devices based on the structure illustrated in Fig. 1 are fabricated. Figure 5 shows the detailed photovoltaic parameters including the open-circuit voltage (V_{oc}), the short-circuit current density (J_{sc}), fill factors (FF), and PCE for the devices with different CH_3NH_3I concentrations. The photovoltaic parameters for those devices are summarized in Table 1. The device without CH_3NH_3I modification exhibits an average PCE of 9.68 % and the best PCE of 10.55 %. After the modification by CH_3NH_3I solution at $x = 10$, the best PCE of PSCs reaches 12.44 %. The device exhibits J_{sc}~20.41 mA/cm^2, V_{oc}~884 mV, and FF~68.01 %, yielding an average PCE of 12.27 %. The CH_3NH_3I modification improves all the device parameters at the optimal concentration of 10 mg/ml. When the concentration of CH_3NH_3I is increased to 20 mg/ml, V_{oc} and FF decrease, leading to lower PCE. This can be attributed to too much excessive CH_3NH_3I caused by the higher concentration, resulting in a redundant impurity to hinder charge transport [27].

Figure 6a presents the *J-V* curves of PSCs without and with CH_3NH_3I modification at $x = 10$. Remarkably, the average PCE increases to 12.27 % after CH_3NH_3I modification. The introduction of the CH_3NH_3I results in significantly enhancement of PCE. The J_{sc} increases from 19.44 to 20.41 mA/cm^2, V_{oc} from 826 to 884 mV, FF from 60.3 to 68.0 %, and the average PCE from 9.68 to 12.27 % for the reference device and modified device at the optimal concentration, respectively. For PSCs, the device performance variation is usually observed from batch to batch. In this work, we have fabricated 28 devices for 7 batches

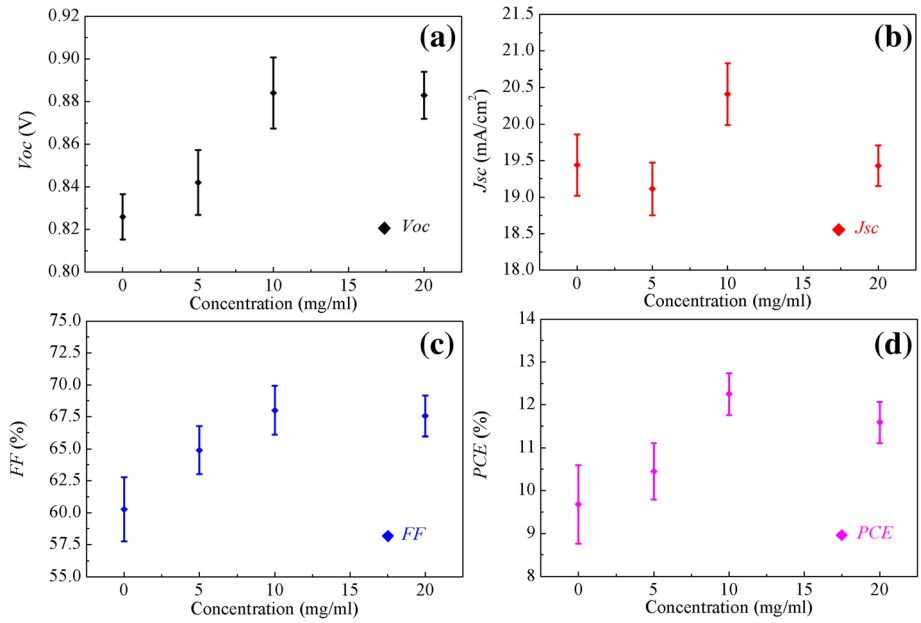

Fig. 5 (Color online) **a** V_{OC}, **b** J_{SC}, **c** FF, and **d** PCE as a function of CH_3NH_3I concentrations for PSCs

to confirm the effect of CH_3NH_3I modification on the performance. Figure 6b shows the statistic histogram of PCE for the device without and with the CH_3NH_3I modification at different concentrations. The device performance of PSCs with CH_3NH_3I modification at the optimal concentration exhibits a narrowed distribution of PCE (range, 11.45 to 12.44 %, with the averaged value of 12.27 %). However, the reference devices show much lower PCE (averaged value 9.68 %) in a wide range (from 8.80 to 10.55 %). Obviously, the improved performance and better reproducibility verified the significance of CH_3NH_3I interfacial modification. The possible mechanisms for the enhanced performance of PSCs will be explored below. To further investigate the origin of the increase of J_{sc}, the absorption spectra and EQE curves for the reference device and modified device by CH_3NH_3I solution at the optimal concentration of 10 mg/ml are presented in Fig. 7, respectively. As shown in Fig. 7, the CH_3NH_3I modification obviously increases the light absorption and EQE in the visible region at the wavelengths less than 600 nm. The enhanced absorbance and EQE contribute to the improvement of J_{sc} in the modified device.

Table 1 The photovoltaic parameters of the PSCs modified by CH_3NH_3I with different concentrations

CH_3NH_3I (mg/ml)	V_{oc} (mV)	J_{sc} (mA/cm^2)	FF (%)	PCE (%)	
				Averaged	Best
0	826	19.44	60.27	9.68	10.55
5	842	19.11	64.90	10.44	11.21
10	884	20.41	68.01	12.27	12.44
20	883	19.43	67.56	11.59	11.97

In order to get a better understanding of the microscopic mechanisms for the observed enhancement of the performance upon the CH_3NH_3I modification, the EIS is carried out to characterize the charge transfer dynamics of PSCs. The Nyquist plots for PSCs measured at −0.8 V (close to V_{oc}) in the dark are presented in Fig. 8a. The solid lines in Fig. 8a are the fits of experimental data using the model in the panel of Fig. 8b. For more accurate fitting, the CPE is used instead of the ideal capacitance C to account for spatial inhomogeneities induced by defects and impurities at the interface. It is can be seen that the measured Nyquist plots can be fitted well by the panel in Fig. 8b. The Nyquist plots consist of two semicircles (See Additional file 1: Figure S1). The first arc at higher frequencies is related to the charge transport and extraction in the Au electrode [30]. The main semicircle is related to the charge recombination at $TiO_2/CH_3NH_3PbI_{3-x}Cl_x$/spiro-OMeTAD interface. Similar results have also been reported in the literature [25, 31–34]. The significant difference can be seen in the Nyquist plots of the PSCs with and without CH_3NH_3I modification. The size of the arc increases with the increase of the concentration of CH_3NH_3I solution and then decreases when the concentration increases to 20 mg/ml, as shown in Fig. 8a. Figure 8c shows the fitted values of the recombination resistance (R_{rec}) for PSCs without and with CH_3NH_3I modification of various concentrations at different bias voltages. It is noted that the device with CH_3NH_3I

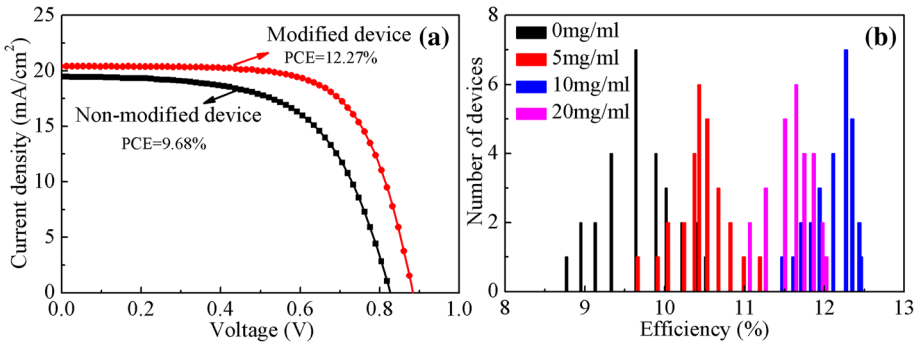

Fig. 6 (Color online) **a** The *J-V* curves of PSCs without and with CH_3NH_3I modification at the optimal concentration ($x = 10$), **b** PCE histogram of PSCs based on meso-TiO_2 film by CH_3NH_3I modification with different concentrations

modification exhibits the higher R_{rec} than the device without CH_3NH_3I modification. It indicates that the recombination rate decreases after the CH_3NH_3I modification because the recombination rate is inversely proportional to R_{rec} [35]. This will benefit for the charge transfer from perovskite to TiO_2 [25]. Because all devices are fabricated at the same process except for the CH_3NH_3I modification, the difference in recombination rate can be attributed to the interface modification of CH_3NH_3I. The device modified by CH_3NH_3I solution at $x = 10$ shows the largest R_{rec} at the same bias voltage, corresponding to the lowest recombination rate. This result is consistent with the variation tendency of the V_{oc} as a function of CH_3NH_3I concentrations. It is notable that V_{oc} is strongly influenced by the recombination rate at the heterojunction of a solar cell [36, 37]. Lower recombination rate in solar cells will lead to a higher V_{oc}. Therefore, the significant improvements of the V_{oc} and the PCE of the PSCs after CH_3NH_3I modification can be understood, which is similar to the effect of surface modification observed in PSCs reported before [23, 31]. Figure 8d shows the plots for the ratio of shunt resistance (R_{sh}) to series resistance (R_s) and FF for the cells modified by CH_3NH_3I solutions with different concentrations. It is reported that the FF depends on the ratio of R_{sh} to R_s [38, 39]. The higher FF value for the cell modified by CH_3NH_3I solution is partially attributed to the large ratio of R_{sh} to R_s. In short, this PSC modified at the optimal process has the highest J_{sc}, V_{oc}, and FF, thus the best performances.

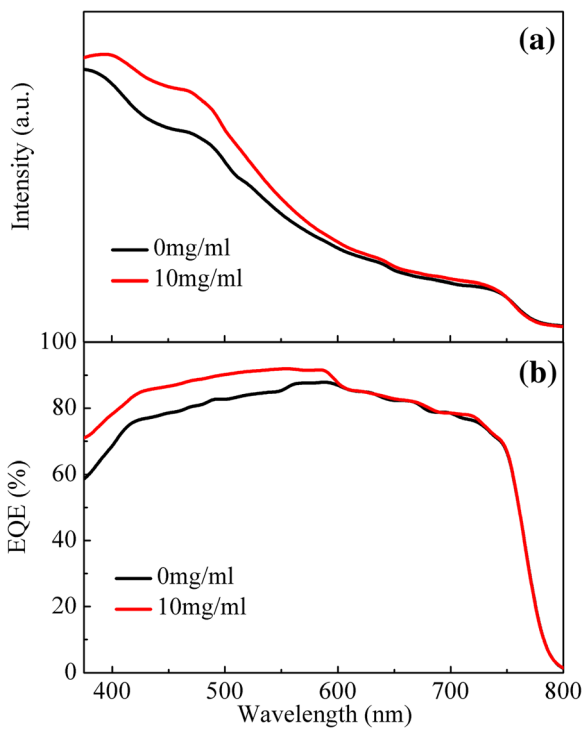

Fig. 7 (Color online) **a** Absorbance and **b** external quantum efficiency (EQE) of PSCs without and with CH_3NH_3I modification at the optimal concentration ($x = 10$)

The PL spectra are usually used to explore the trap states and recombination properties of light-excited charge in semiconductors [23, 40–42]. Figure 9 shows the PL spectra of $CH_3NH_3PbI_{3-x}Cl_x$ films deposited on bare TiO_2 and modified TiO_2 by CH_3NH_3I solutions with different concentrations. It can be seen that the peak position of the emission is consistent for all of the samples. However, their PL intensities vary a lot and increase with increase of the CH_3NH_3I concentration from 0 to 10 mg/ml, then decrease when the concentration increases to 20 mg/ml. The $CH_3NH_3PbI_{3-x}Cl_x$ film deposited on bare TiO_2 exhibits the highest intensity in PL spectra, corresponding to a higher charge recombination [23]. The $CH_3NH_3PbI_{3-x}Cl_x$ film deposited on modified TiO_2 by CH_3NH_3I with the concentration of 10 mg/ml shows the lowest peak intensity, indicating the lowest recombination rate [42] and thus the best

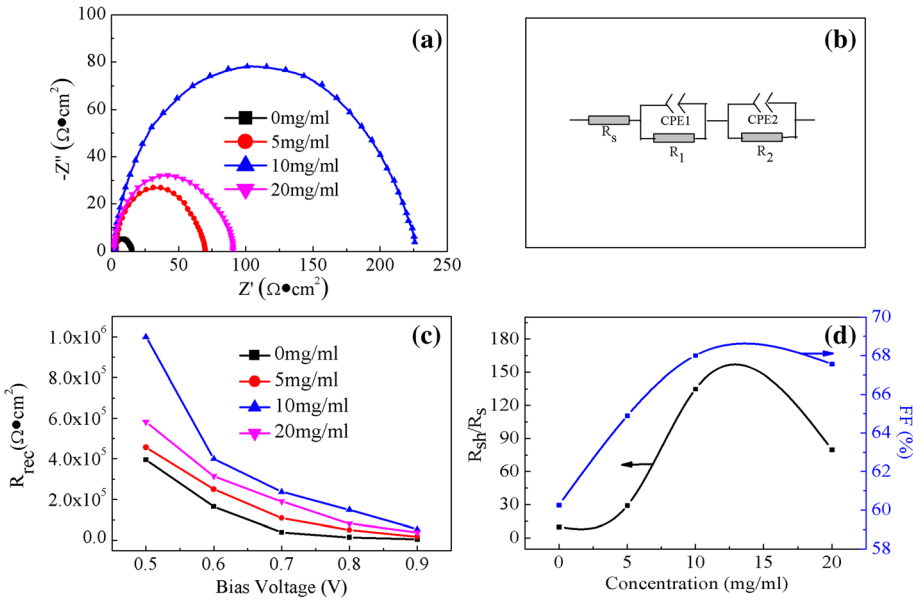

Fig. 8 (Color online) **a** Nyquist plots of PSCs modified by CH_3NH_3I solution with different concentrations measured at the bias voltage of −0.8 V (close to V_{oc}) in the dark, **b** Equivalent circuit employed to fit the Nyquist plots. *Solid lines* in **a** are the fittings of the experimental data using the model in panels **b** and **c**. Recombination resistance (R_{rec}) of PSCs obtained from **b** as a function of concentrations for CH_3NH_3I. **d** The ratio of shunt resistance (R_{sh}) to series resistance (R_s) and FF as a function of concentrations for CH_3NH_3I

photovoltaic performance. This is consistent with the results obtained in EIS characterization (Fig. 8). It confirms that the CH_3NH_3I modification on the TiO_2 layer results in the reduction of recombination rate at the interface between the TiO_2 and $CH_3NH_3PbI_{3-x}Cl_x$. The reduced recombination rate of photogenerated charges at the interface can contribute to the enhanced charge collection efficiency in the PSCs, resulting in the improved performance.

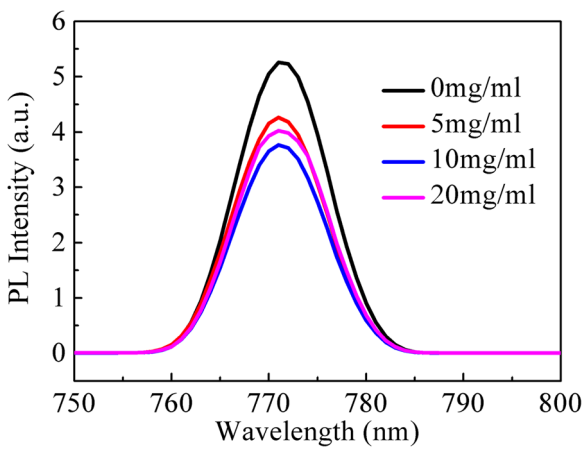

Fig. 9 (Color online) Photoluminescence spectra of $CH_3NH_3PbI_{3-x}Cl_x$ film deposited on meso-TiO_2 films modified by CH_3NH_3I solution with different concentrations

Conclusions

In summary, a series of PSCs based on the structure of glass/FTO/compact TiO_2/meso-TiO_2/$CH_3NH_3PbI_{3-x}Cl_x$/spiro-OMeTAD/Ag have been fabricated. CH_3NH_3I are used to modify the interface between meso-TiO_2 and $CH_3NH_3PbI_{3-x}Cl_x$. It has been revealed that modifying the interface by CH_3NH_3I with appropriate concentration can significantly improve the performance of PSCs. After the CH_3NH_3I modification, the PCE of PSCs increases to 12.27 from 9.68 % of the references device. It is suggested that the better performance for CH_3NH_3I modified device is mainly attributed to the improved crystalline property, increased sunlight absorption in the visible range and reduced charge recombination rate.

Additional file

Additional file 1: Figure S1. The Nyquist plots of PSCs modified by CH_3NH_3I solution with different concentrations, measured at the bias voltage of −0.8 V (close to V_{oc}) in the dark. The polts in (a) and (c) correspond to the amplified spectra of (b) and (d) in the high frequency range, respectively. The two R-CPE circuits in series are employed to fit the experimental data in (a) and (b). Only one R-CPE circuit is used to fit the data in (c) and (d). The solid lines are the fittings of the experimental data. It can be seen that the experimental data can be better fitted in Figure S1(a) and S1(b) than that in Figure S1(c) and S1(d). This confirms that the Nyquist plots consist of two semicircles. (TIF 168 kb)

Competing interests
The authors declare that they have no competing interests.

Authors' contributions
SJW proposed the idea and designed the experiments. WW performed the experiments, analyzed results, and drafted the manuscript. ZBZ, YYC, JSC, JMW, and RYH participated in the sample fabrication and characterizations. XSG, XBL, and LLS contributed to the data interpretation. SJW and JML contributed to the data interpretation, manuscript writing, and supervised the research. All authors read and approved the final manuscript.

Acknowledgements
We acknowledge the financial support of the National Natural Science Foundation of China (Grant No. 51431006, 61271127, 51472093, 21303060,61574065), Guangdong Natural Science Foundation (2016A030313421), Guangdong Engineering Technology Center of Optofluidics Materials and Devices (2015B090903079), International Science and Technology Cooperation Platform Program of Guangzhou (No. 2014 J4500016), the State Key Program for Basic Researches of China (Grant No. 2015CB921202), the Project for Guangdong Province Universities and Colleges Pearl River Scholar Funded Scheme (2014), Science and Technology Planning Project of Guangdong Province (2015B090927006), and Program for Changjiang Scholars and Innovative Research Team in University (IRT13064).

Author details
[1]Institute for Advanced Materials and Laboratory of Quantum Engineering and Quantum Materials, South China Normal University, Guangzhou 510006, China. [2]South China Academy of Advanced Optoelectronics, South China Normal University, Guangzhou 510006, China. [3]Laboratory of Solid State Microstructures, Nanjing University, Nanjing 210093, China.

Received: 29 March 2016 Accepted: 24 June 2016
Published online: 29 June 2016

References

1. Kojima A, Teshima K, Shirai Y, Miyasaka T (2009) Organometal halide perovskites as visible-light sensitizers for photovoltaic cells. J Am Chem Soc 131(17):6050–6051
2. Xing GC, Mathews N, Sun SY, Lim SS, Lam YM, Grätzel M, Mhaisalkar S, Sum TC (2013) Long-range balanced electron- and hole-transport lengths in organic-inorganic $CH_3NH_3PbI_3$. Science 342(6156):344–347
3. Im JH, Lee CR, Lee JW, Park SW, Park NG (2011) 6.5 % efficient perovskite quantum-dot-sensitized solar cell. Nanoscale 3(10):4088–4093
4. Bi DQ, Tress W, Dar MI, Gao P, Luo JS, Renevier C, Schenk K, Abate A, Giordano F, Baena JPC, Decoppet JD, Zakeeruddin SM, Nazeeruddin MK, Grätzel M, Hagfeldt A (2016) Efficient luminescent solar cells based on tailored mixed-cation perovskites. Sci Adv 2(1):e1501170
5. Liu MZ, Johnston MB, Snaith HJ (2013) Efficient planar heterojunction perovskite solar cells by vapour deposition. Nature 501(7467):395–398
6. Yang WS, Noh JH, Jeon NJ, Kim YC, Ryu SC, Seo J, Seok SI (2015) High-performance photovoltaic perovskite layers fabricated through intramolecular exchange. Science 348(6240):1234–1237
7. Liu DY, Kelly TL (2014) Perovskite solar cells with a planar heterojunction structure prepared using room-temperature solution processing techniques. Nat Photon 8(2):133–138
8. Liang PW, Liao CY, Chueh CC, Zuo F, Williams ST, Xin XK, Lin JJ, Jen AKY (2014) Additive enhanced crystallization of solution-processed perovskite for highly efficient planar-heterojunction solar cells. Adv Mater 26(22):3748–3754
9. Eperon GE, Burlakov VM, Docampo P, Goriely A, Snaith HJ (2014) Morphological control for high performance, solution-processed planar heterojunction perovskite solar cells. Adv Funct Mater 24(1):151–157
10. Wu CG, Chiang CH, Tseng ZL, Nazeeruddin MK, Hagfeldt A, Grätzel M (2015) High efficiency stable inverted perovskite solar cells without current hysteresis. Energy Environ Sci 8(9):2725–2733
11. Yu H, Wang F, Xie FY, Li WW, Chen J, Zhao N (2014) The role of chlorine in the formation process of "$CH_3NH_3PbI_{3-x}Cl_x$" perovskite. Adv Funct Mater 24(45):7102–7108
12. Jeon NJ, Noh JH, Kim YC, Yang WS, Ryu S, Seok SI (2014) Solvent engineering for high-performance inorganic-organic hybrid perovskite solar cells. Nat Mater 13(9):897–903
13. Singh T, Miyasaka T (2016) High performance perovskite solar cell via multi-cycle low temperature processing of lead acetate precursor solutions. Chem Commun 52:4784–4787
14. Troughton J, Carnie MJ, Davies ML, Charbonneau C, Jewell EH, Worsley DA, Watson TM (2016) Photonic flash-annealing of lead halide perovskite solar cells in 1 ms. J Mater Chem A 4(9):3471–3476
15. Liu TF, Jiang FY, Tong JH, Qin F, Meng W, Jiang YY, Li ZF, Zhou YH (2016) Reduction and oxidation of poly(3,4-ethylenedioxythiophene): poly(styrenesulfonate) induced by methylamine (CH_3NH_2)-containing atmosphere for perovskite solar cells. J Mater Chem A 4:4305–4011
16. Zhou HP, Chen Q, Li G, Luo S, Song TB, Duan HS, Hong ZR, You JB, Liu YS, Yang Y (2014) Interface engineering of highly efficient perovskite solar cells. Science 345(6196):542–546
17. Chandiran AK, Nazeeruddin MK, Grätzel M (2014) The role of insulating oxides in blocking the charge carrier recombination in dye-sensitized solar cells. Adv Funct Mater 24(11):1615–1623
18. Sun Z, Liang M, Chen J (2015) Kinetics of iodine-free redox shuttles in dye-sensitized solar cells: interfacial recombination and dye regeneration. Acc Chem Res 48(6):1541–1550
19. Azimi H, Ameri T, Zhang H, Hou Y, Quiroz COR, Min J, Hu MY, Zhang ZG, Przybilla T, Matt GJ, Spiecker E, Li YF, Brabec CJ (2015) A universal interface layer based on an amine-functionalized fullerene derivative with dual functionality for efficient solution processed organic and perovskite solar cells. Adv Energy Mater 5(8):1401692
20. Li X, Dar MI, Yi CY, Luo JS, Tschumi M, Zakeeruddin SM, Nazeeruddin MK, Han HW, Grätzel M (2015) Improved performance and stability of perovskite solar cells by crystal crosslinking with alkylphosphonic acid ω-ammonium chlorides. Nat Chem 7:703–711
21. Li WZ, Zhang W, Reenen SV, Sutton RJ, Fan JD, Haghighirad AA, Johnston MB, Wang LD, Snaith HJ (2016) Enhanced UV-light stability of planar heterojunction perovskite solar cells with caesium bromide interface modification. Energy Environ Sci 9:490–498
22. Liu LF, Mei AY, Liu TF, Jiang P, Sheng YS, Zhang LJ, Han HW (2015) Fully printable mesoscopic perovskite solar cells with organic silane self-assembled monolayer. J Am Chem Soc 137(5):1790–1793
23. Zuo LJ, Gu ZW, Ye T, Fu WF, Wu G, Li HY, Chen HZ (2015) Enhanced photovoltaic performance of $CH_3NH_3PbI_3$ perovskite solar cells through interfacial engineering using self-assembling monolayer. J Am Chem Soc 137(7):2674–2679
24. Zhang SH, Zuo LJ, Chen JH, Zhang ZQ, Mai JQ, Lau TK, Lu XH, Shi MM, Chen HZ (2016) Improved photon-to-electron response of ternary blend organic solar cells with a low band gap polymer sensitizer and interfacial modification. J Mater Chem A 4:1702–1707
25. Shih YC, Wang LY, Hsieh HC, Lin KF (2015) Enhancing the photocurrent of perovskite solar cells via modification of the $TiO_2/CH_3NH_3PbI_3$ heterojunction interface with amino acid. J Mater Chem A 3(17):9133–9136
26. Marin-Beloqui JM, Lanzetta L, Palomares E (2015) Decreasing charge losses in perovskite solar cells through the mp-TiO_2/MAPI interface engineering. Chem Mater 28(1):207–213
27. Yantara N, Yanan F, Shi C, Dewi HA, Boix PP, Mhaisalkar SG, Mathews N (2015) Unravelling the effects of Cl addition in single step $CH_3NH_3PbI_3$ perovskite solar cells. Chem Mater 27(7):2309–2314
28. Xie Y, Shao F, Wang YM, Xu T, Wang DL, Huang FQ (2015) Enhanced performance of perovskite $CH_3NH_3PbI_3$ solar cell by using CH_3NH_3I as additive in sequential deposition. ACS Appl Mater Interfaces 7(23):12937–12942
29. Conings B, Baeten L, Dobbelaere CD, Haen JD, Manca J, Boyen HG (2014) Perovskite-based hybrid solar cells exceeding 10 % efficiency with high reproducibility using a thin film sandwich approach. Adv Mater 26(13):2041–2046
30. Li WZ, Dong HP, Guo XD, Li N, Li JW, Niu GD, Wang LD (2014) Graphene oxide as dual functional interface modifier for improving wettability and retarding recombination in hybrid perovskite solar cells. J Mater Chem A 2: 20105–20111
31. Yu JC, Kim DB, Baek G, Lee BR, Jung ED, Lee S, Chu JH, Lee DK, Choi KJ, Cho S, Song MH (2015) High-performance planar perovskite optoelectronic devices: a morphological and interfacial control by polar solvent treatment. Adv Mater 27(23):3492–3500
32. Zohar A, Kedem N, Levine I, Zohar D, Vilan A, Ehre D, Hodes G, Cahen D (2016) Impedance spectroscopic indication for solid state electrochemical reaction in $(CH_3NH_3)PbI_3$ films. J Phys Chem Lett 7(1):191–197
33. Miyano K, Tripathi N, Yanagida M, Shirai Y (2016) Lead halide perovskite photovoltaic as a model p–i–n diode. Acc Chem Res 49(2):303–310
34. Sabba D, Agarwala S, Pramana SS, Mhaisalkar S (2014) A maskless synthesis of TiO_2-nanofiber-based hierarchical structures for solid-state dye-sensitized solar cells with improved performance. Nanoscale Res Lett 9:14

35. Fabregat-Santiago F, Garcia-Belmonte G, Mora-Seró I, Bisquert J (2011) Characterization of nanostructured hybrid and organic solar cells by impedance spectroscopy. Phys Chem Chem Phys 13(20):9083–9118
36. Rau U (2007) Reciprocity relation between photovoltaic quantum efficiency and electroluminescent emission of solar cells. Phys Rev B 76(8):085303
37. Wu SJ, Li JH, Lo SC, Tai QD, Yan F (2012) Enhanced performance of hybrid solar cells based on ordered electrospun ZnO nanofibers modified with CdS on the surface. Org Electron 13(9):1569–1575
38. Gershon TS, Sigdel AK, Marin AT, van Hest MFAM, Ginley DS, Friend RH, MacManus-Driscoll JL, Berry JJ (2013) Improved fill factors in solution-processed ZnO/Cu_2O photovoltaics. Thin Solid Films 536:280–285
39. Sze SM, Ng KK (2006) Physics of semiconductor devices. Wiley interscience; John Wiley & Sons
40. Marco ND, Zhou HP, Chen Q, Sun PY, Liu ZH, Meng L, Yao EP, Liu YS, Schiffer A, Yang Y (2016) Guanidinium: a route to enhanced carrier lifetime and open-circuit voltage in hybrid perovskite solar cells. Nano Lett 16(2):1009–1016
41. Chen LC, Chen JC, Chen CC, Wu CG (2015) Fabrication and properties of high-efficiency perovskite/PCBM organic solar cells. Nanoscale Res Lett 10:312
42. Nejand BA, Ahmadi V, Gharibzadeh S, Shahverdi HR (2016) Cuprous oxide as a potential low-cost hole-transport material for stable perovskite solar cells. ChemSusChem 9(3):302–313